Journal of Metals, Materials and Minerals, Vol. 32, No. 4, pp. 79-86, 2022

Development of Fe_xO_y particle onto bacterial cellulose network by forced hydrolysis and its electrical conductivity

Prompong KHAMWONGS[1], Poramed WONGJOM[2], Andi Magattang Gafur MUCHLIS[3,4], Chun Che LIN[3,4,*], Seranee SRISUK[1], and Sarute UMMARTYOTIN[1,*]

[1] *Department of Materials and Textile Technology, Faculty of Science and Technology, Thammasat University, Patumtani, 12120, Thailand*
[2] *Department of Physics, Faculty of Science and Technology, Thammasat University, Patumtani, 12120, Thailand*
[3] *Institute of Organic and Polymeric Materials, National Taipei University of Technology, Taipei, 106344, Taiwan*
[4] *Research and Development Center for Smart Textile Technology, National Taipei University of Technology, Taipei, 106344, Taiwan*

***Corresponding author e-mail:** sarute@tu.ac.th, cclin0530@mail.ntut.edu.tw

Received date:
21 August 2022
Revised date
21 September 2022
Accepted date:
29 September 2022

Keywords:
Bacterial cellulose;
Iron(III) chloride;
Composite;
Conductivity

Abstract

FexOy particle and bacterial cellulose composite sheet was successfully prepared by forced hydrolysis. The presence of Fe3+ ions in bacterial cellulose suspension significantly provided the positive charge due to electrostatic force as reported by Zeta potential. With the pH of 12 of bacterial cellulose suspension, particle was nucleated between bacterial cellulose networks. Fourier transform infrared exhibited Fe-O stretching. X-ray diffraction reported that the mixture of Fe_2O_3 and Fe_3O_4 was existed onto bacterial cellulose composite. Scanning electron microscope reported that Fe_xO_y particle was randomly distributed in bacterial cellulose network. Intensity of Fe was qualitatively observed by energy dispersive analysis. With the existence of Fe_xO_y particle, the composite illustrated the inferiority of thermal stability of 150°C. Furthermore, it was noted that the resistivity was reduced with respect to increment of Fe_xO_y particle, suggesting that electrical conductivity was then enhanced. It was remarkable to note that Fe_xO_y particle and bacterial cellulose composite sheet prepared from forced hydrolysis showed the excellent properties as a candidate for flexible electrode.

1. Introduction

Nowadays, the electronics industry was extremely attracted in various sectors of research because of electronic devices were very important to help in facilitating daily use. The role of electronics was well-known in a wide variety of applications such as telecommunication devices, generator and battery. Electronic devices can be designed for use in applications such as mobile phones, televisions and energy materials [1]. Although electronic devices significantly provided numerous benefits in order to facilitate the daily life, they were still limited due to shot lifespan [2]. Novel apparatus will be replaced in order to maintain the performance during usage. As a result, it was consequently created the electronic waste. Electronic waste was typically considered as a hazardous material. The disposal process was still un able to control the efficiency. It was thus harmful to environment. It may cause a trouble to the soil, groundwater and air [2,3]. As a consequence, it was affected to health risk such as skin allergic, respiration failure and immune system disorders.

Up to the present time, one of the most attractive strategies for waste management was to replace with bio-based materials. It was considered as an effective route to environmental remediation such as waste reduction, less consumption of hazardous chemical reagent and ecologically controllable emission. Moreover, the utilization of bio-based materials was typically related to "Green policies" [4]. This policy was extremely encouraged on the use of eco-friendly raw materials and process which minimize the hazardous chemical reagent. In response to "Green policies", utilization of cellulose as bio-based material was therefore favorable. To the best of authors knowledge, it was remarkable to note that cellulose was considered as one of the most naturally occurring bio-based materials. It can be found in plant and certain bacteria. From the structural point of view, it was presented as a long-chain polysaccharide composed of β(1→4) glycosidic bond of a cellulose unit. It offered chemical resistance as well as high temperature resistance [5]. With outstanding properties of cellulose, it was therefore employed to be a reinforcing for bio-based composite. It enrolled in numerous sectors of application such as medical technology, colorimetric and electrochemical sensor as well as flexible electronic[6].

One of the most important sources is focused on "bacterial cellulose". It can be prepared by fermentation process of *Acetobacter Xylinum Bacteria* and reverse engineering process of food waste. It was notable that bacterial cellulose provided the advantage of high purity [7]. It is free from wax, lignin and hemicellulose [8]. Furthermore, bacterial cellulose was structural defined as a nano-fibrous network. It offered the superiority of mechanical properties compared to plant based cellulosic materials. Furthermore, in order to develop as a flexible electronic substrate, although bacterial cellulose significantly offered excellent mechanical properties, it was still limited on electrical

conductivity. Therefore, to enhance the electrical conductivity of bacterial cellulose was extremely developed. One way to improve the electrical conductivity was to add metal ions into solution. Ferric chloride ($FeCl_3$) was considered as one of the most effective chemical reagents. It can be effectively dissociated into Fe^{3+} ion adhered onto hydroxyl group of cellulose network [9]. It can be thus resulted in electrical conductivity enhancement [10].

In 2012, Ummartyotin *et al.* [11] studied the role of bacterial cellulose sheet composite as a substrate electronic device. It was observed that composite provided the great promise in high transparency, high thermal resistance and excellent flexibility. After that, Ummartyotin *et al.* [12] also found that modified bacterial cellulose by grafting with strontian ion can be effectively enhanced the electroactive properties. Recently, in 2022, Sun *et al.* [13] developed polypyrrole and $SnCl_2$ modified bacterial cellulose as a flexible electrode for supercapacitor. It exhibited a capacitance of 5718 $mF{\cdot}cm^{-2}$ at a current density of 0.5 $mA{\cdot}cm^{-2}$. Bharti *et al.* [14] investigated the role of bacterial cellulose as an electrode for battery. It illustrated that bacterial cellulose presented uniform interface for efficient redox reaction. It can be used for long term of battery cycle.

From the viewpoint of synthetic strategy, bacterial cellulose can be employed as a nano-particle formation. This concept was conducted based on thermodynamic equilibrium and nucleation growth. In 2019, Phutanon *et al.* [15] evaluated the task of bacterial cellulose as a template for CuO particle on bacterial cellulose sheet. CuO particle was nucleated by forced hydrolysis within bacterial cellulose network. It can be employed as photocatalyst material and antimicrobial agent. In 2022, Robić *et al.* [16] investigated the forced hydrolysis of $FeCl_3$ solution by the existence of guanylurea phosphate. This technique was considered as an effective route in order to prepare giniite ($Fe_5(PO_4)_4(OH)_3{\cdot}2H_2O$). It can be designed to be a single-phase with various particle shapes.

To use bacterial cellulose-based composite for electronic device, electrical properties were considered as one of an important way to develop. One way to enhance these properties was to integrate Fe_3O_4 particle onto bacterial cellulose sheet. In 2020, Dacrory *et al.* [17] developed a flexible film composite from cyanoethyl cellulose (CEC) and magnetite (Fe_3O_4). With the existence of Fe_3O_4, bacterial cellulose composite exhibited the paramagnetic behavior under an external applied magnetic field. Yang *et al.* [18] developed Fe_3O_4 and cellulose composite for UV sensor. Fe_3O_4 was presented in between cellulose network. It significantly provided the magnetic properties.

In order to enhance the electrical conductivity of bacterial cellulose-based composite, bacterial cellulose was employed as a bio-template for Fe_3O_4 formation by forced hydrolysis of $FeCl_3$. From the fundamental point of view, Fe^{3+} ions accepted the OH ions of water and formed on the bacterial cellulose sheet. It can offer the excellent uniformity and dispersion of Fe_xO_y particle onto bacterial cellulose network. The range of pH was investigated for Fe_xO_y particle formation onto bacterial cellulose sheet. Fourier-transform infrared spectroscopy (FTIR) and X-ray diffraction (XRD) were employed to evaluate the functional group and crystallinity, respectively. Scanning electron microscopy (SEM) and energy dispersive X-ray spectroscopy (EDX) were used to study the morphology and distribution of element. Thermal degradation behavior was evaluated by thermogravimetric analysis (TGA). After that electrical conductivity was then reported.

2. Experimental

2.1 Materials

Bacterial cellulose was successfully extracted from a commercial *nata de coco* product, which is locally produced in Thailand. *Nata de coco* is a dessert, in which the main component is bacterial cellulose. Premium grade sodium hydroxide was purchased from Emsure, Sigma Aldrich, Co., Ltd. Iron (III) chloride hexahydrate and ammonia were purchased from Daejung Chemicals and Metals, Co., Ltd., Republic of Korea and Alfa Aesar, Co., Ltd., People's Republic of China, respectively. Both were used to enhance the electrical conductivity of bacterial cellulose. All chemical reagents were used as received without further purifications.

2.2 Methods

2.2.1 Bacterial cellulose extraction and purification.

Bacterial cellulose was extracted from *nata de coco*. It was washed several times with distilled water in order to remove syrup and impurities. Then, it was blended in a laboratory blender in order to obtain lower size. After that *nata de coco* was treated in 2% w/v of NaOH solution at 80°C for 3 h to remove impurity. For solvent removal, the suspension was filtrated by suction flask with connected to vacuum pump. Then, it was consequently cleansed with distilled water until neutral pH. Bacterial cellulose suspension was stored in refrigerator. The process of cellulose extraction is provided in Figure 1(a). Addition information of cellulose extraction and purification was similar to our previous article [19].

2.2.2 Development of Fe_xO_y and bacterial cellulose sheet composites.

10, 20, 30, 40, and 50 wt% of $FeCl_3$ were added into the bacterial cellulose suspension. It was continuously stirred for 1 h in order to ensure the homogeneity. Then, the ammonia solution was dropped until pH of 12 was obtained. The mixture was stirred for 1 h. After that, the water is removed from the suspension through a Buchner funnel filter equipped with a membrane filter, polytetrafluoroethylene membrane (mesh 0.1 μm, diameter 120 mm), connected to the Buchner flask and vacuum pump. The composite volume was adjusted to obtain a dry weight of 1 g of the composite. The schematic diagram Fe_xO_y and bacterial cellulose sheet composites is presented in Figure 1(b).

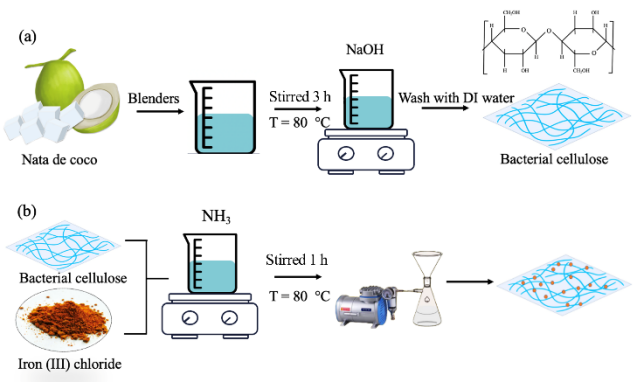

Figure. 1 (a) Bacterial cellulose extraction and purification and (b) Development of $FeCl_3$ and bacterial cellulose sheet composites.

2.3 Characterization

2.3.1 Fourier-transform infrared spectroscopy (FTIR)

The Fourier-transform infrared (FT-IR) spectra were measured using a Thermal Scientific Nicolet iS5 spectrometer with scanning wavenumber from 4000 cm^{-1} to 500 cm^{-1}. It was operated with a resolution of ±4 cm^{-1} and a scan frequency of 32 times.

2.3.2 X-ray diffraction

The X-ray diffraction (XRD) patterns were obtained by using a Bruker AXS D8 advanced diffractometer with Cu Kα radiation (λ = 1.54 Å) at 40 kV and 35 mA. The diffraction pattern was recorded over a range of 5° to 60°. The step was set at 2°·min^{-1}.

2.3.3 Scanning electron microscopy

The appearance and interface of the obtained samples after air-drying were characterized by Scanning electron microscopy (JEOL, JFC-1200) combined with Energy-dispersive spectroscopy (EDS) mapping. The magnification of 40000X and accelerating voltage of 2 kV were employed.

2.3.4 Thermogravimetric analysis

The TGA characteristics were investigated by TGA. Each sample was heated at a heating rate of 10°·min^{-1} under nitrogen atmosphere from room temperature to 600°C

2.3.5 Dynamic light scattering

The particle size was investigated by using "particle size analyzer". The model was ZetaSizer Nano ZS, Malvern Instruments, Ltd., UK). Clear disposable zeta cell was employed. The refractive index was 1.47. Water was employed as a dispersant. The sample was prepared as 10 μL by diluted in 2 mL of DI water.

2.3.6 Four point probe resistivity

A four-point probe is a simple apparatus for measuring the resistivity of semiconductor samples. By passing a current through two outer probes and measuring the voltage through the inner probes allows the measurement of the substrate resistivity. The doping concentration can be calculated from the resistivity using the formulas discussed in the appendices and the PV Lighthouse Resistivity Calculator

Ohm's law $V = IR$

First law of resistance $R = \rho L/A$

3. Results and discussion

3.1 Investigation of Fe_xO_y in bacterial cellulose suspension sheet by force hydrolysis

Fe_xO_y was successfully synthesized by using bacterial cellulose sheet as a template. It was homogeneously nucleated at the free space between bacterial cellulose chain. No significant change of properties of bacterial cellulose were observed compared to pristine bacterial cellulose sheet. The color of bacterial cellulose suspension was changed from whitish to orange color. This was probably due to the color of Fe^{3+} ion. This was similar to previous literature of Bai e*t al.* [10]. From the fundamental point of view, $FeCl_3$ was dissolved into bacterial cellulose suspension. It was dissociated into Fe^{3+} ion and Cl^- ion, respectively. The Fe^{3+} ion can be adhered with the hydroxyl group alongside of bacterial cellulose network by electrostatic force. Or, it can be formed to be $Fe(OH)_3$ by the presence of ammonia. This structure exhibited instability as suggested by Majzlan *et al.* [20]. It was therefore formed Fe_xO_y particle within bacterial cellulose network. The formations of Fe_xO_y particle within bacterial cellulose were presented in equation (1) and (2), respectively.

$$FeCl_3 + NH_4OH \rightarrow Fe(OH)_3 + NH_4Cl \quad (1)$$

$$Fe(OH)_3 \rightarrow Fe_xO_y \text{ particle} \quad (2)$$

In Fe^{3+} and bacterial cellulose suspension, it was presented as a colloidal particle of bacterial cellulose fiber. In order to evaluate the formation of Fe_xO_y particle within bacterial cellulose network, Zeta potential was considered as an important strategy for colloidal stability determination. Table 1 reports the zeta potential of Fe_xO_y particle in bacterial cellulose suspension. The range of data was reported to be 30 mV to 60 mV. It can be indicated that Fe_xO_y particle was uniformly distributed. It exhibited outstanding properties of colloidal stability. The positive data was due to the presence of Fe^{3+} in suspension. Furthermore, the charge was still increased in positive way with respect to the amount of Fe_xO_y particle [21]. However, in case of pristine bacterial cellulose, the range of zeta potential was reported as negative data. It can be adhered with Fe^{3+} ion onto bacterial cellulose network. It was similar to previous literature of Robic *et al.* [16].

3.2 Evaluation of Fe_xO_y and bacterial cellulose composite sheet

Fe_xO_y and bacterial cellulose composite sheet was successfully prepared from forced hydrolysis technique. All of samples exhibited as a flat sheet. The color of sheet was changed from whitish to orange color, similar to its suspension state. With presence of Fe_xO_y particle, composite was still in paper sheet form. It was remarkable to note that all samples were easily adsorbed by humidity. It should be stored in desiccator in order to prevent water absorption.

Table 1. Zeta potential analysis of the Fe_xO_y and bacterial cellulose suspension.

Sample	Zeta potential (mV)
Bacterial cellulose (BC)	-40.6
10 wt% Fe_xO_y/BC	38.5
20wt% Fe_xO_y/BC	46.9
30 wt% Fe_xO_y/BC	51.4
40 wt% Fe_xO_y/BC	55.8
50 wt% Fe_xO_y/BC	61.1

In order to determine the functional group of Fe_xO_y and bacterial cellulose-based composite, Fourier-transform infrared spectroscopy (FTIR) was employed. Pristine cellulose was provided for comparison. Figure 2 exhibits the FTIR spectra of Fe_xO_y and bacterial cellulose-based composites. All of samples showed the similar characteristic feature. It was observed that the wavenumber of 1064 cm^{-1} and 1640 cm^{-1} were presented. They were corresponded to C-O stretching and C=C stretching, respectively. This was in agreement with previous work of Phutanon *et al.* [15]. These functional group were belonged to β(1→4) linked D-glucose units of bacterial cellulose. For the Fe^{3+} grafted onto hydroxyl group of bacterial cellulose, no significant change on functional group of bacterial cellulose was observed. Moreover, the characteristic peak at the wavenumber of 3400 cm^{-1} was observed. It was attributed to O-H stretching of bacterial cellulose. This functional group may create the H-bonding formation by adhered with water molecule. Furthermore, it may use to modify by grafting with Fe^{3+}. It may create the bonding formation throughout bacterial cellulose network, as suggested by Xi *et al.* [22]. The addition of Fe^{3+} resulted in a decrease in the hydrogen bonds. Only side group was successfully modified. In addition, the characteristic peak at the wavenumber of 584 cm^{-1} was observed. It was corresponded to Fe-O stretching [23]. Significant evidence was observed compared to pristine bacterial cellulose. However, it was controversial that the peak of 1647 cm^{-1} was observed. It regarded as the formation of the C=O bond when $FeCl_3$ was added. It was noted that the double bond was unstable and easily to be oxidized. Fe^{3+} ions exhibited strong oxidizing properties. It was subsequently inferred that the presence of the C=O bond made the electrode reaction faster, resulting in larger reaction rate constant and charge transfer coefficient [24].

In order to determine the crystallinity of Fe_xO_y and bacterial cellulose-based composite, X-ray diffraction technique was therefore employed. Figure 3 illustrates the X-ray diffraction patterns of Fe_xO_y and bacterial cellulose composite. Investigation of neat bacterial cellulose sheet was provided for comparison. It was observed that the characteristic peaks of 2 theta of 14.5°, 16.5° and 22.5° were presented. They were corresponded to diffraction plane of [101], [010] and [020], respectively. They were indexed to cellulose. These Miller planes were associated with previous literature of Kumar *et al.* [25]. Furthermore, with the presence of Fe_xO_y particle, the peak related to the mixture of Fe_2O_3 and Fe_3O_4 was typically observed. It was remarkable to note that the position of Fe_2O_3 was presented at the diffraction angle of 12° and 27°. Due to small portion of Fe_xO_y, the intensities were still less compared to pristine bacterial cellulose, as suggested by literature of Kumar *et al.* [26]. On the other hand, the diffraction peak at 35° was presented, this peak was typically related to the existence of Fe_3O_4 particle, as suggested by literature of Patwa *et al.* [27]. With the occurrence of Fe_xO_y, the crystallinity of bacterial cellulose was still similar [26]. The Fe_xO_y particle was located onto the surface of bacterial cellulose and/or it may present throughout bacterial cellulose network. However, the intensities were still less, it resulted in the interference onto the diffraction plane of pristine bacterial cellulose. Although Fe_xO_y and bacterial cellulose composite sheet was successfully prepared by forced hydrolysis technique, it provided the difficulty to control the phase and composition of Fe_2O_3 and Fe_3O_4 in bacterial cellulose network.

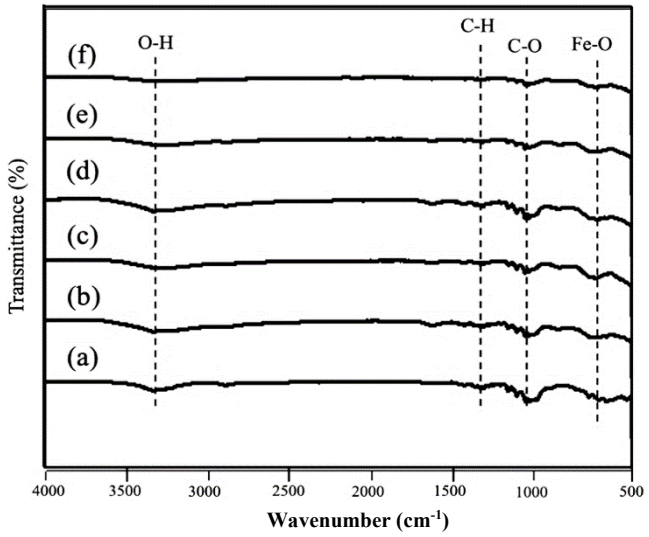

Figure 2. FTIR spectra of the Fe_xO_y and bacterial cellulose-based composites: ((a) bacterial cellulose sheet, (b) 10 wt% Fe_xO_y and bacterial cellulose-based composites, (c) 20 wt% Fe_xO_y and bacterial cellulose-based composites, (d) 30 wt% Fe_xO_y and bacterial cellulose-based composites, (e) 40 wt% Fe_xO_y and bacterial cellulose-based composites, and (f) 50 wt% Fe_xO_y and bacterial cellulose-based composites.

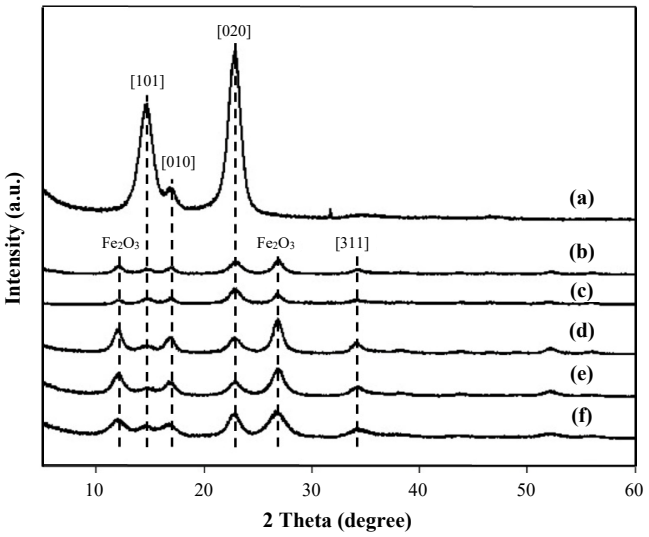

Figure 3. XRD pattern of the Fe_xO_y and bacterial cellulose-based composites: (a) bacterial cellulose sheet, (b) 10 wt% Fe_xO_y and bacterial cellulose-based composites, (c) 20 wt% Fe_xO_y and bacterial cellulose-based composites, (d) 30 wt% Fe_xO_y and bacterial cellulose-based composites, (e) 40 wt% Fe_xO_y and bacterial cellulose-based composites, and (f) 50 wt% Fe_xO_y and bacterial cellulose-based composites.

In order to determine the morphological properties of Fe_xO_y and bacterial cellulose composite, a scanning electron microscope was employed. This technique allowed us to investigate the microstructure of Fe_xO_y and bacterial cellulose composite. Figure 4 exhibits the morphological properties of the Fe^{3+} and bacterial cellulose-based composites. Microstructure of neat bacterial cellulose was provided for comparison. With the presence of Fe_xO_y particle, no significant change of morphology was observed. It exhibited as a randomly fiber network of bacterial cellulose. This is identical to previous literature

of Chanthiwong *et al.* [28]. The size of bacterial cellulose was estimated to be 10 nm to 100 nm. The size of bacterial cellulose network can be used to predict the size of Fe_xO_y with confined geometry. It was expected to form the cluster located throughout bacterial cellulose network. It may form van der Waals interaction between hydroxyl group of bacterial cellulose and Fe^{3+} charge [29]. With the presence of Fe_xO_y, the image become clearer. This may imply that Fe^{3+} was sensitive to electron beam during investigation. Furthermore, the porosity was occurred in between bacterial cellulose network. It was created due to the repulsive force of hydroxyl group among bacterial cellulose networks.

In order to ensure the presence of Fe_xO_y onto bacterial cellulose sheet, elemental analysis by energy dispersive analysis was employed. This strategy allowed us to determine the presence of Fe atom onto bacterial cellulose sheet. Figure 5 presents the qualitative analysis by EDX technique. The sample was still similar to SEM investigation with different area of observation. It was remarkable to note that two distinct peaks of oxygen and carbon were observed with high intensity. These peaks were corresponded to β-1,4 linked D-glucose unit of cellulose. It can be used to confirm that carbon and oxygen atoms were the main component of composite sheet. Furthermore, with the presence of Fe_xO_y, intensity of Fe was observed, as suggested by Zhang *et al.* [30]. This was very evident compared to pristine bacterial cellulose sheet. The intensity of Fe observed by EDX implied that Fe_xO_y was formed by forced hydrolysis technique. This experiment was in agreement with XRD.

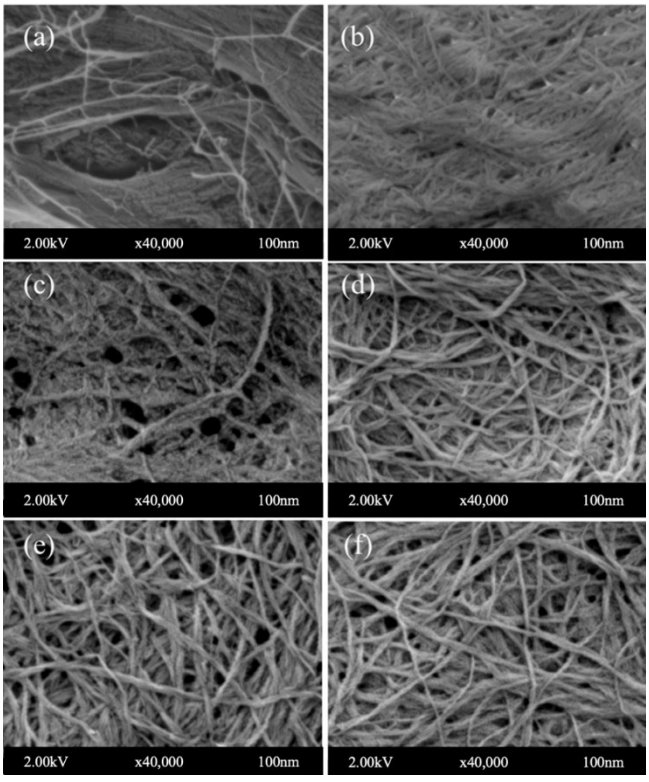

Figure 4. Morphological properties of the Fe_xO_y and bacterial cellulose-based composites (a) bacterial cellulose sheet, (b) 10 wt% Fe_xO_y and bacterial cellulose-based composites, (c) 20 wt% Fe_xO_y and bacterial cellulose-based composites, (d) 30 wt% Fe_xO_y and bacterial cellulose-based composites, (e) 40 wt% Fe_xO_y and bacterial cellulose-based composites, and (f) 50 wt% Fe_xO_y and bacterial cellulose-based composites.

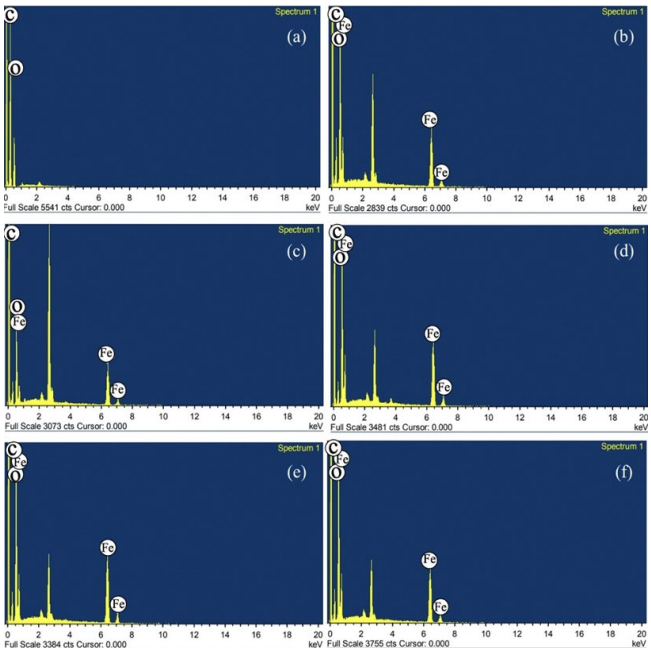

Figure 5. Elemental analysis of the Fe^{3+} and bacterial cellulose-based composites: (a) bacterial cellulose sheet, (b) 10 wt% Fe_xO_y and bacterial cellulose-based composites, (c) 20 wt% Fe_xO_y and bacterial cellulose-based composites, (d) 30 wt% Fe_xO_y and bacterial cellulose-based composites, (e) 40 wt% Fe_xO_y and bacterial cellulose-based composites, and (f) 50 wt% Fe_xO_y and bacterial cellulose-based composites.

In order to determine the thermal decomposition of Fe_xO_y and bacterial cellulose composite, thermogravimetric analysis technique was employed. Figure 6 exhibits the thermal decomposition of Fe_xO_y and bacterial cellulose composite. Neat bacterial cellulose was provided for comparison. It was notable that thermal decomposition characteristic was presented in the similar feature. It can be classified into three different region of weight loss. From ambient temperature to 150°C, only 7% to 13% of weight loss was observed due to water evaporation. It was remarkable to note that to use Fe_xO_y and bacterial cellulose composite as an electronic substrate, to avoid the moisture absorption should be considered. It may provide the damage to electric circuit. After that, within the temperature range of 150°C to 500°C, broad region of weight loss was observed. It was estimated to be 36% to 47% of weight loss. It was typically referred to pyrolysis of bacterial cellulose sheet. It may change from organic structure to volatile gas such as CO_2. Furthermore, when the temperature was increased up to 600°C, the percent of weight loss was constant [26]. It can be indicated that thermal degradation was completely occurred. No pyrolysis was observed within this temperature region. It was presented as a char and residual. However, comparing to thermal decomposition of neat bacterial cellulose, the feature of curve was different. The presence of Fe_xO_y particle may induce on oxidizing ability for bacterial cellulose sheet. The first region of weight loss was observed from room temperature to 200°C. Only 10 wt% of weight loss was observed due to water evaporation. It was notable that although Fe_xO_y particle significantly provided the enhancement of electrical properties, it may offer lower thermal stability. The broad region of weight loss was reported to be 74 wt% within the temperature region of 200°C to 500°C. It involved to pyrolysis of bacterial cellulose. This was in agreement with previous work of Fan *et al.* [31]. Then, when the

temperature was elevated to 600°C, weight loss was constant. Only 20 wt% of weight loss was observed. It was typically referred to char and residual.

3.3 Preliminary investigation of electrical conductivity

In order to design as flexible bioelectrode, the electrical conductivity was investigated. This property allowed us to determine the feasibility of Fe_xO_y and bacterial cellulose-based composite for electrode. Four points probe technique was employed to measure the resistivity. The pristine bacterial cellulose sheet was also investigated. It exhibited high resistivity, similar to many previous works [32,33]. It was remarkable to note that bacterial cellulose exhibited low electrical conductivity and high dielectric strength. Furthermore, in case of composite, significant reduction of resistivity was observed with respect to increment of $FeCl_3$. The range of resistivity was observed between 50 kΩ to 300 kΩ. The variation of resistivity level was occurred due to the position of Fe_xO_y particle. It can imply that non-uniformity and distribution were presented. Furthermore, to be the flexible electrode, the conductivity level may report. It was notable that with the existence of $FeCl_3$, it was changed to Fe_xO_y by forced hydrolysis technique. The electrical conductivity was then enhanced. With the presence of electrical conductivity, it was remarkable to note that Fe_xO_y and bacterial cellulose-based composite was considered as an excellent candidate for electrode.

Table 2 reports the electrical conductivity and application of cellulose-based composite. The range of electrical conductivity was versatile depending on metal oxide and conductive polymer within cellulose network. It can be used to predict the possibility of application such as sensor and semiconductor. The Fe_xO_y and bacterial cellulose-based composite illustrated the similar level of electrical conductivity of flexible electrode. It therefore remarkably offered the excellent potential for being as a candidate for the flexible electrode in the near future.

4. Conclusion

Fe_xO_y and bacterial cellulose composite sheet was successfully prepared by forced hydrolysis. The role of pH of 12 was controllable by aid of ammonia. It can initiate the heterogeneous nucleation of Fe_xO_y particle throughout bacterial cellulose network. With the increment on Fe^{3+} ions in bacterial cellulose suspension, the positive data of zeta potential was increased with respect to positive charge of Fe^{3+} ions. It referred to excellent colloidal stability. Fe-O stretching was also confirmed by FTIR. The mixture of Fe_2O_3 and Fe_3O_4 onto surface of bacterial cellulose was investigated XRD. Bacterial cellulose network was illustrated as random orientation. Fe_xO_y was inserted between its nano-network. It was qualitatively indicative by EDX that intensity of Fe was occurred. It can be thermally stable within 150°C, as observed by TGA. With the increment of Fe_xO_y particle, the resistivity was continuously reduced. It can be reported that electrical conductivity was therefore increased. It can be concluded that Fe_xO_y and bacterial cellulose composite sheet presented attractive properties for being as a candidate of "Green electrode".

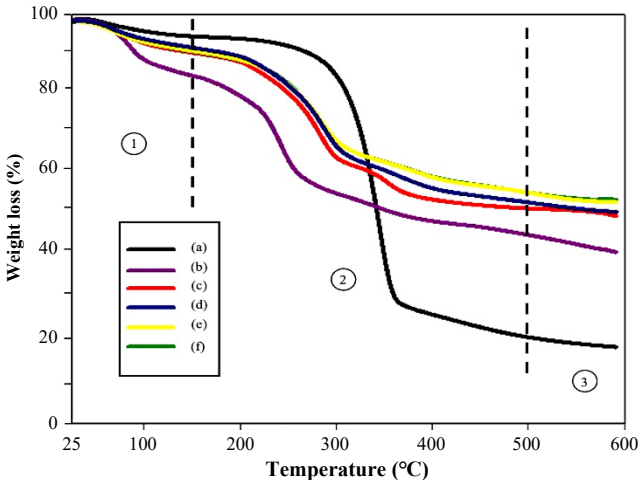

Figure 6. TGA of the Fe^{3+} and bacterial cellulose-based composites: (a) bacterial cellulose sheet, (b) 10 wt% Fe_xO_y and bacterial cellulose-based composites, (c) 20 wt% Fe_xO_y and bacterial cellulose-based composites, (d) 30 wt% Fe_xO_y and bacterial cellulose-based composites, (e) 40 wt% Fe_xO_y and bacterial cellulose-based composites, and (f) 50 wt% Fe^{3+} and bacterial cellulose composite.

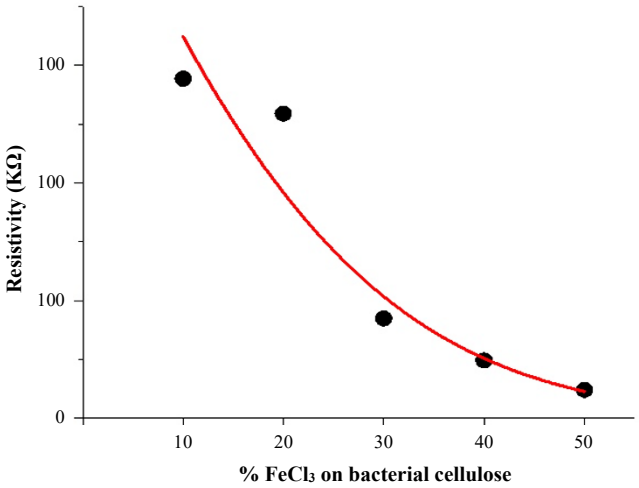

Figure 7. Resistivity of the Fe_xO_y and bacterial cellulose-based composites.

Table 2. Comparison of conductivity levels of conductive cellulose composites.

Materials	Conductivity level (S/cm)	Application	References
PAM/CNC-g-PVP/rGO-g-PAA	8.3×10^{-4}	Flexible strain sensors	[34]
Ionic conductive hydroxypropyl methyl cellulose reinforced hydrogels (PAM/HPMC/LiCl)	9.82	Sensitive skin-like sensors	[35]
PVA/CNF-AgNWs	3.57×10^{-2}	Flexible electronics	[36]
Cellulose nano whiskers, polypyrrole, AgNP assisted with NiO NP	$2.5 \times 10^{-11} – 1.1 \times 10^{-7}$	Semiconductor	[37]
Cellulose-based dialdehyde and carboxyl with Fe^{3+}	N/A	Sensor	[38]
Fe_xO_y and bacterial cellulose-based composite	$5 \times 10^{-2} – 3 \times 10^{-1}$	Flexible electrode	This work

Acknowledgement

This work was supported by the National Science and Technology Council of Taiwan (contract nos. NSTC 110-2113-M-027-012, NSTC 110-2622-M-027-001, and NSTC 111-2113-M-027-005-MY2), and Joint International Cooperation Program Funding by National Taipei University of Technology and Thammasat University (Contract Nos. NTUT-TU-110-02).

This study was supported by Matching Fund Between Thammasat University Research Fund and National Taipei University of Technology, Contract No. MF 1/2564. The authors would like to acknowledge Thammasat University Research Unit in Textile and Polymer Chemistry.

References

[1] S. Saleem, M. H. Jameel, A. Rehman, M. B. Tahir, M. I. Irshad, Z.-Y. Jiang, R. Q. Malik, A. A. Hussain, A. ur Rehman, A. H. Jabbar, A. Y. Alzahrani, M. A. Salem, and M. M. Hessien, "Evaluation of structural, morphological, optical, and electrical properties of zinc oxide semiconductor nanoparticles with microwave plasma treatment for electronic device applications," *Journal of Materials Research and Technology,* vol. 19, pp. 2126-2134, 2022.

[2] M. U. Bukhari, A. Khan, K. Q. Maqbool, A. Arshad, K. Riaz, and A. Bermak, "Waste to energy: facile, low-cost and environment-friendly triboelectric nanogenerators using recycled plastic and electronic wastes for self-powered portable electronics," *Energy Reports,* vol. 8, pp. 1687-1695, 2022.

[3] X. Pan, C. W. Wong, and C. Li, "Circular economy practices in the waste electrical and electronic equipment (WEEE) industry: A systematic review and future research agendas," *Journal of Cleaner Production,* p. 132671, 2022.

[4] D. Fullerton, and W. Wu, "Policies for green design," *Journal of environmental economics and management,* vol. 36, no. 2, pp. 131-148, 1998.

[5] D. Zamel, and A. U. Khan, "Bacterial immobilization on cellulose acetate based nanofibers for methylene blue removal from wastewater: Mini-review," *Inorganic Chemistry Communications,* vol. 131, p. 108766, 2021.

[6] K. Jin, C. Jin, and Y. Wu, "Synthetic biology-powered microbial co-culture strategy and application of bacterial cellulose-based composite materials," *Carbohydrate Polymers,* p. 119171, 2022.

[7] J. Wang, J. Tavakoli, and Y. Tang, "Bacterial cellulose production, properties and applications with different culture methods–A review," *Carbohydrate polymers,* vol. 219, pp. 63-76, 2019.

[8] R. R. Singhania, A. K. Patel, Y-S. Tseng, V. Kumar, C-W. Chen, D. Haldar, J. K. Saini, and C-D. Dong, "Developments in bioprocess for bacterial cellulose production," *Bioresource Technology,* vol. 344, p. 126343, 2022.

[9] J. Li, W. Liu, J. Meng, L. Zhao, J. Li, and M. Zheng, "Mesothermal pretreatment using FeCl3 enhances methane production from rice straw," *Renewable Energy,* vol. 188, pp. 670-677, 2022.

[10] H. Bai, D. Chen, H. Zhu, S. Zhang, W. Wang, P. Ma, and W. Dong "Photo-crosslinking ionic conductive PVA-SbQ/$FeCl_3$ hydrogel sensors," *Colloids and Surfaces A: Physicochemical and Engineering Aspects,* vol. 648, p. 129205, 2022.

[11] S. Ummartyotin, J. Juntaro, M. Sain, and H. Manuspiya, "Development of transparent bacterial cellulose nanocomposite film as substrate for flexible organic light emitting diode (OLED) display," *Industrial crops and products,* vol. 35, no. 1, pp. 92-97, 2012.

[12] S. Ummartyotin, S. Thiangtham, and H. Manuspiya, "Strontium-modified bacterial cellulose and a polyvinylidene fluoride composite as an electroactive material," *Forest Products Journal,* vol. 67, no. 3-4, pp. 288-296, 2017.

[13] Y. Sun, Y. Yang, L. Fan, W. Zheng, D. Ye, and J. Xu, "Polypyrrole/$SnCl_2$ modified bacterial cellulose electrodes with high areal capacitance for flexible supercapacitors," *Carbohydrate Polymers,* p. 119679, 2022.

[14] V. K. Bharti, A. D. Pathak, C. S. Sharma, and M. Khandelwal, "Flexible and free-standing bacterial cellulose derived cathode host and separator for lithium-sulfur batteries," *Carbohydrate Polymers,* p. 119731, 2022.

[15] N. Phutanon, K. Motina, Y.-H. Chang, and S. Ummartyotin, "Development of CuO particles onto bacterial cellulose sheets by forced hydrolysis: A synergistic approach for generating sheets with photocatalytic and antibiofouling properties," *International journal of biological macromolecules,* vol. 136, pp. 1142-1152, 2019.

[16] M. Robić, M. Ristić, S. Krehula, and S. Musić, "Forced hydrolysis of $FeCl_3$ solutions in the presence of guanylurea phosphate," *Colloids and Surfaces A: Physicochemical and Engineering Aspects,* vol. 634, p. 128047, 2022.

[17] S. Dacrory, M. Moussa, G. Turky, and S. Kamel, "In situ synthesis of Fe_3O_4@ cyanoethyl cellulose composite as antimicrobial and semiconducting film," *Carbohydrate polymers,* vol. 236, p. 116032, 2020.

[18] W. Yang, H. Tian, J. Liao, Y. Wang, L. Liu, L. Zhang, and A. La, "Flexible and strong Fe_3O_4/cellulose composite film as magnetic and UV sensor," *Applied Surface Science,* vol. 507, p. 145092, 2020.

[19] L. Sakwises, N. Rodthongkum, and S. Ummartyotin, "SnO_2- and bacterial-cellulose nanofiber-based composites as a novel platform for nickel-ion detection," *Journal of Molecular Liquids,* vol. 248, pp. 246-252, 2017.

[20] J. Majzlan, A. Navrotsky, and U. Schwertmann, "Thermodynamics of iron oxides: Part III. Enthalpies of formation and stability of ferrihydrite (~$Fe(OH)_3$), schwertmannite (~$FeO(OH)_3$/ $4(SO_4)1/8$), and ε-Fe_2O_3 1 1Associate editor: D. Wesolowski," *Geochimica et Cosmochimica Acta,* vol. 68, no. 5, pp. 1049-1059, 2004.

[21] P. P. Gopmandal, and J. F. L. Duval, "Electrostatics and electrophoresis of engineered nanoparticles and particulate environmental contaminants: beyond zeta potential-based formulation," *Current Opinion in Colloid & Interface Science,* p. 101605, 2022.

[22] Y. Xi, T. Xie, Y. Liu, Y. Wu, H. Liu, Z. Su, Y. Huang, X. Yuan, C. Zhang, and X. Li, "Carboxymethyl cellulose stabilized ferrous sulfide@extracellular polymeric substance for Cr(VI) removal: Characterization, performance, and mechanism," *Journal of Hazardous Materials,* vol. 425, p. 127837, 2022.

[23] Y. Chen, P. Pötschke, J. r. Pionteck, B. Voit, and H. Qi, "Fe_3O_4 nanoparticles grown on cellulose/GO hydrogels as advanced catalytic materials for the heterogeneous Fenton-like reaction," *ACS omega,* vol. 4, no. 3, pp. 5117-5125, 2019.

[24] J. Xu, Q. Ma, H. Su, F. Qiao, P. Leung, A. A. Shah, and Q. Xu, "Redox characteristics of iron ions in different deep eutectic solvents," *Ionics,* vol. 26, no. 1, pp. 483-492, 2020.

[25] A. Kumar, Y. S. Negi, V. Choudhary, and N. K. Bhardwaj, "Characterization of cellulose nanocrystals produced by acid-hydrolysis from sugarcane bagasse as agro-waste," *Journal of materials physics and chemistry,* vol. 2, no. 1, pp. 1-8, 2014.

[26] B. Kumar, R. Priyadarsh, Sauraj, F. Deeba, A. Kulshreshtha, K. K. Gaikwad, J. Kim, A. Kumar, and Y. S. Negi, "Nanoporous sodium carboxymethyl cellulose-g-poly (Sodium acrylate)/$FeCl_3$ hydrogel beads: Synthesis and characterization," *Gels,* vol. 6, no. 4, p. 49, 2020.

[27] R. Patwa, O. Zandraa, Z. Capáková, N. Saha, and P. Sáha, "Effect of iron-oxide nanoparticles impregnated bacterial cellulose on overall properties of alginate/casein hydrogels: Potential injectable biomaterial for wound healing applications," *Polymers,* vol. 12, no. 11, p. 2690, 2020.

[28] M. Chanthiwong, W. Mongkolthanaruk, S. J. Eichhorn, and S. Pinitsoontorn, "Controlling the processing of co-precipitated magnetic bacterial cellulose/iron oxide nanocomposites," *Materials & Design,* vol. 196, p. 109148, 2020.

[29] L. Chaabane, H. Chaabane, R. Mehdaoui, M. Snoussi, E. Beyou, M. Lahcini, and M. H. V. Baouab, "Functionalization of developed bacterial cellulose with magnetite nanoparticles for nano-biotechnology and nanomedicine applications," *Carbohydrate Polymers,* vol. 247, p. 116707, 2020.

[30] Z. J. Zhang, and X. Y. Chen, "Carbon nanofibers derived from bacterial cellulose: Surface modification by polydopamine and the use of ferrous ion as electrolyte additive for collaboratively increasing the supercapacitor performance," *Applied Surface Science,* vol. 519, p. 146252, 2020.

[31] K. Fan, T. Zhang, S. Xiao, H. He, J. Yang, and Z. Qin, "Preparation and adsorption performance of functionalization cellulose-based composite aerogel," *International Journal of Biological Macromolecules,* vol. 211, pp. 1-14, 2022.

[32] S. Jeon, Y.-M. Yoo, J.-W. Park, H.-J. Kim, and J. Hyun, "Electrical conductivity and optical transparency of bacterial cellulose based composite by static and agitated methods," *Current Applied Physics,* vol. 14, no. 12, pp. 1621-1624, 2014.

[33] G. Liu, M. Ma, H. Meng, J. Liu, Y. Zheng, J. Peng, S. Wei, Y. Sun, Y. Wang, Y. Xie, and J. Li, "In-situ self-assembly of bacterial cellulose/poly(3,4-ethylenedioxythiophene)-sulfonated nanofibers for peripheral nerve repair," *Carbohydrate Polymers,* vol. 281, p. 119044, 2022.

[34] B. Li, Y. Chen, Y. Han, X. Cao, and Z. Luo, "Tough, highly resilient and conductive nanocomposite hydrogels reinforced with surface-grafted cellulose nanocrystals and reduced graphene oxide for flexible strain sensors," *Colloids and Surfaces A: Physicochemical and Engineering Aspects,* p. 129341, 2022.

[35] Z. Qin, S. Liu, J. Bai, J. Yin, N. Li, and T. Jiao, "Ionic conductive hydroxypropyl methyl cellulose reinforced hydrogels with extreme stretchability, self-adhesion and anti-freezing ability for highly sensitive skin-like sensors," *International Journal of Biological Macromolecules,* vol. 220, pp. 90-96, 2022.

[36] B. A. Widyaningrum, P. Amanda, D. A. Pramasari, R. S. Ningrum, W. Kusumaningrum, Y. D. Kurniawan, A. N. Amenaghawon, H. Darmokoesoemo, and H. Kusuma, "Preparation of a conductive cellulose nanofiber-reinforced pva composite film with silver nanowires loading," *Nano-Structures & Nano-Objects,* vol. 31, p. 100904, 2017.

[37] A. M. El-Nahrawy, A. B. Abou Hammad, T. A. Khattab, A. Haroun, and S. Kamel, "Development of electrically conductive nanocomposites from cellulose nanowhiskers, polypyrrole and silver nanoparticles assisted with Nickel(III) oxide nanoparticles," *Reactive and Functional Polymers,* vol. 149, p. 104533, 2020.

[38] Y. Wang, H. Zhang, H. Zhang, J. Chen, B. Li, and S. Fu, "Synergy coordination of cellulose-based dialdehyde and carboxyl with Fe^{3+} recoverable conductive self-healing hydrogel for sensor," *Materials Science and Engineering: C,* vol. 125, p. 112094, 2021.